



## D 4.1 PARAMETRIC STUDY ON SLAT NOISE REDUCTION AND SELECTION OF BEST NRTS BASED ON POROUS TREATMENTS

<b>Document authors</b>			
Hasan Kamliya Jawahar, Mahdi Azarpeyvand		UoB	
<b>Document contributors</b>			
Christophe Schram Matthias Meinke Daniele Ragni Gareth Bennet	VKI RWTH TUD TCD	Michael Pott-Pollenske Eric Manoha Vincent Fleury	DLR ONERA DAV

### Abstract


In this report, the results from the experimental studies of slat noise reduction using porous materials carried out at the Aeroacoustic wind tunnel of the University of Bristol are reported. The porous slat inserts fitted on DLR's F16 two-element high-lift device with modified trailing edge were tested for angles of attack of  $AoA=16^\circ$ ,  $18^\circ$  and  $20^\circ$  at freestream velocities of  $U = 30\text{m/s}$  and  $U = 37\text{m/s}$ . The results show that the use of porous material within the slat cavity does not significantly reduce the slat noise. However, a very mild noise reduction between 3-5 kHz was observed for the slat with porous treatments. This noise reduction is hypothesized to be due to the reduction in acoustic reflection from the lower side of the slat.

### Keywords

Slat noise reduction, porous materials.

## Information Table

Project information	
<b>PROJECT ID</b>	860538
<b>PROJECT FULL TITLE</b>	INnoVative dEsign of iNstalled airframe componenTs for aircraft nOise Reduction
<b>PROJECT ACRONYM</b>	INVENTOR
<b>FUNDING SCHEME</b>	RIA – Research and Innovation Action
<b>START DATE OF THE PROJECT</b>	1st May 2020
<b>DURATION</b>	48 months
<b>CALL IDENTIFIER</b>	H2020-MG-2018-2019-2020

Deliverable information	
<b>DELIVERABLE No AND TITLE</b>	D 4.1 Parametric study on slat noise reduction and selection of best NRTs based on porous treatments
<b>TYPE OF DELIVERABLE<sup>1</sup></b>	Report
<b>DISSEMINATION LEVEL<sup>2</sup></b>	Public
<b>BENEFICIARY NUMBER AND NAME</b>	13 University of Bristol (UoB)
<b>AUTHORS</b>	Hasan Kamliya Jawahar, Mahdi Azarpeyvand
<b>CONTRIBUTORS</b>	Christophe Schram (VKI), Matthias Meinke (RWTH), Daniele Ragni (TUD), Gareth Bennet (TCD), Michael Pott-Pollenske (DLR), Eric Manoha (ONERA), Vincent Fleury (DAV)
<b>WORK PACKAGE No</b>	4
<b>WORK PACKAGE LEADER WP LEADER VALIDATION DATE</b>	02/11/2022
<b>COORDINATOR VALIDATION DATE</b>	25/12/2022
<b>Coordinator signature</b>	Eric MANOHA 

<sup>1</sup> Use one of the following codes: R=Document, report (excluding the periodic and final reports)

DEM=Demonstrator, pilot, prototype, plan designs

DEC=Websites, patents filing, press & media actions, videos, etc.

OTHER=Software, technical diagram, etc.

<sup>2</sup>Use one of the following codes: PU=Public, fully open, e.g. web

CO=Confidential, restricted under conditions set out in Model Grant Agreement

CI=Classified, information as referred to in Commission Decision 2001/844/EC.

# Table of Contents

- 1 Experimental setup .....4
  - 1.1 Model and Instrumentation. ....4
  - 1.2 Test Facility .....5
- 2 Results and discussion .....7
  - 2.1 Static pressure measurements.....7
  - 2.3 Far-field acoustic measurements..... 12
  - 2.4 Near-field Surface pressure measurements..... 16
  - 2.5 Beamforming measurements.....21
- 4 Conclusion .....24



# 1 Experimental setup

## 1.1 Model and Instrumentation.

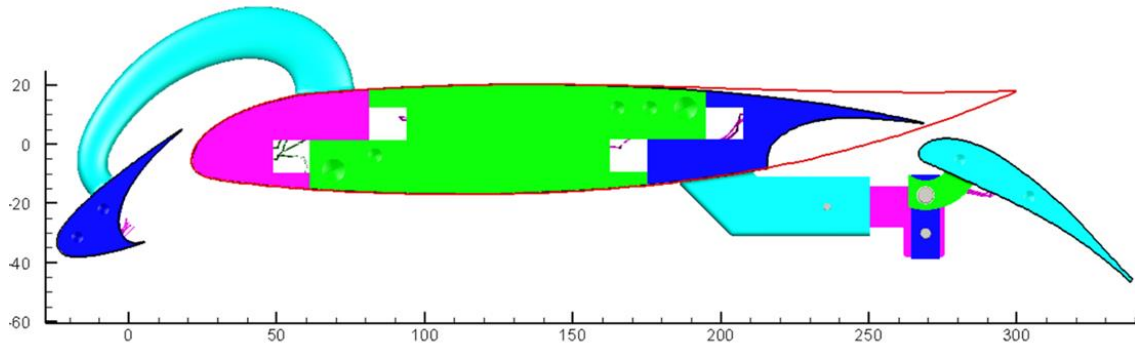


Figure 1 - F16 with modified trailing-edge used in the present study

The existing DLR unswept F16 model was modified to have the trailing edge replaced with a “Valiant-like” trailing edge for tests at UoB. The details of the wing model with the modification have been detailed in report D2.3 by NLR and also in D2.5 by UoB. The modifications to the DLR F16 model are shown in Fig. 1. The F16 model is instrumented with several pressure ports and unsteady pressure sensors. As shown in Fig. 2, a total of 12 Kulite surface pressure transducers were placed on the F16 model. In order to investigate the noise reduction capability of the porous slat inserts, the model was equipped with a cavity on the lower surface of the slat where the porous materials could be inserted (please refer to D2.5). The porous material selection, porous material characteristics, and manufacturing strategy were detailed in D2.5. A total of five porous inserts in the slat and a solid baseline slat insert were used in the present study. This includes DLR-Foam, TUD-Fine, TUD-Medium, TUD-Large, and TCD-Fabric.

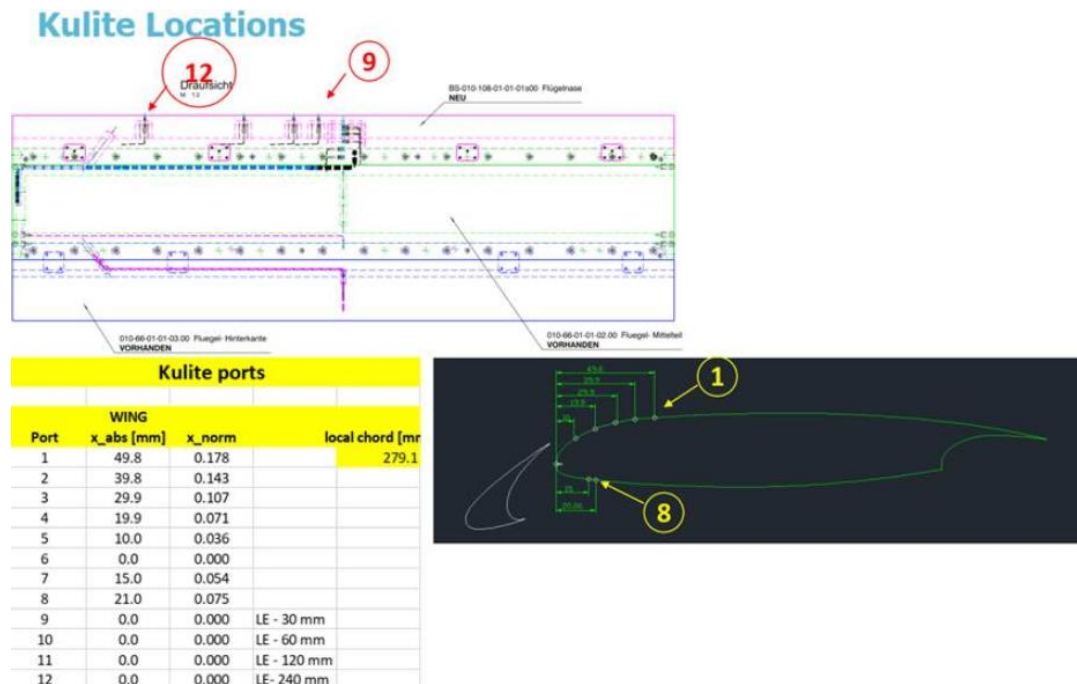


Figure 2 - Location of the unsteady pressure measurement probes on the airfoil.

## 1.2 Test Facility

The aeroacoustic measurements were carried out at the University of Bristol Aeroacoustics Wind Tunnel Facility. As seen in Fig.3, the open jet anechoic wind tunnel is equipped with a Kevlar-walled test section to reduce the effects of flow deflection while maintaining acoustic transparency. The total length of the test section is 1500 mm, leaving a distance of approximately 1700 mm to the inlet plane of the collector. There is a 3.2 m gap between the nozzle outlet and the collector inlet.

The length of the tensioned Kevlar cloth is long enough such that all noise from the aerofoil passes through the Kevlar and not any wind tunnel free shear layer until the noise reaches the far-field directional microphone array. Moreover, considering the length of the Kevlar section in the UoB facility, the effect of the boundary layer will be minimal. The distance from the end of the test section to the collector allows the jet to sufficiently expand before it is channelled into the first silencer after the collector and hence ensures the regenerative noise of the silencer does not exceed the present background noise. The test section shares its internal dimensions of 775 mm in height and 500 mm in width with the exit dimensions of the nozzle of the aeroacoustic facility.

The structure of the section is made from Bosch Rexroth struts and connectors, and the flow-wetted surface area of any strut is smooth and without any mounting slots to avoid any erroneous noise sources. Three windows made from Perspex and Sapele wood are located on each side and the Perspex of the first window has a circular cut-out with a diameter of 500 mm to mount the test object via a side plate. Additionally, the inside of the circular cut-out is lined with 0.1 mm thick PTFE Teflon tape by 3M, to reduce the friction between the side plate and the window. The 300 mm long second and third windows allow the insertion of intrusive measurement techniques, such as hot-wire anemometry.

All windows are sealed on all four sides by means of polychloroprene rubber (Neoprene) strips, which are compressed when installing each window, and hence no air leakages can occur. Furthermore, all internal gaps as well as the connection to the wind tunnel nozzle have been covered with insulation tape to ensure no spurious noise from any steps or gaps is created. The aerodynamic and aeroacoustic tests are carried out for free-stream velocities ranging from 20 to 40m/s.

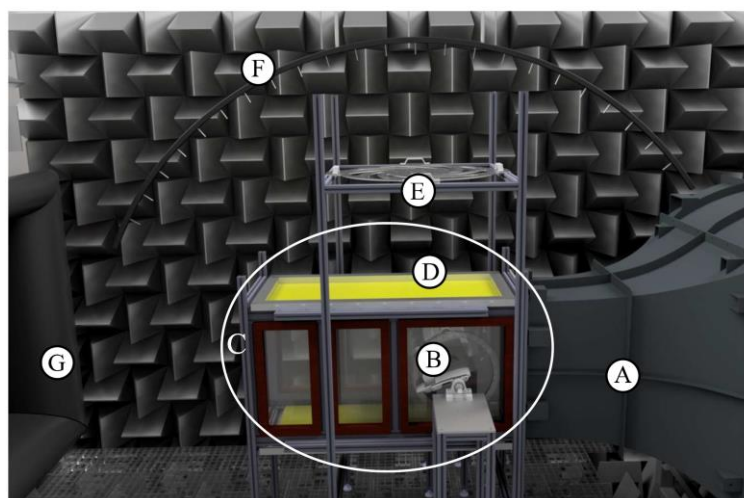
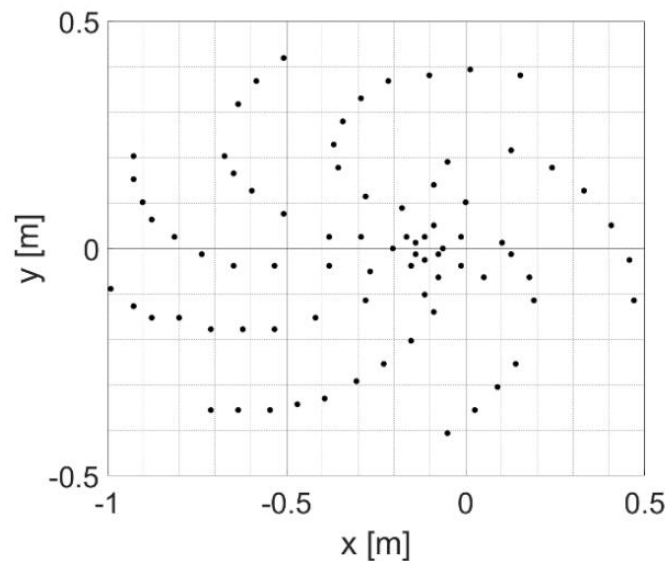


**Figure 3: Overview of the Kevlar-walled test section with the mounted high-lift device inside the anechoic chamber; (A) contraction nozzle, (B) Modified F16 high-lift device, (C) test section, (D) Kevlar tensioning frame, (E) beamforming array, (F) far-field microphone arc, (G) collector.**

To capture the noise generated by the aerofoils, a beamforming array was used, mounted above the Kevlar test section, as illustrated in Fig. 4. The beamforming array consists of a rectangular wire mesh which was equipped with Panasonic WM-61A microphones with a dynamic response from 100Hz to 12000Hz. A concentric elliptic spiral distribution of 80 microphones was designed following an optimization process, using equal-area ellipses to follow the established literature. The microphone array was mounted to the support structure using a mesh grid which allows for the future modification of the array distribution if desired. The additional microphones located at the center allow direct measurements of the noise, as well as correlation with the near-field pressure signals if the noise is sufficiently high compared to the background noise. For the present study, the center of the beamforming array was aligned at the wing trailing edge and positioned at a distance of 1 m above the test section. For maximum transparency, the microphone supports were manufactured using wire mesh, as shown in Fig. 4.



(a)



(b)

**Figure 4: (a) beamforming array mounted above Kevlar-walled test section within anechoic wind tunnel facility, and (b) beamforming array microphone distribution.**

The directivity measurements of the slat noise sources from the F16 airfoil were acquired using a microphone array on a circular arc. The directivity arc, as shown in Fig. 5, consists of 16 G.R.A.S. 40PL microphones located at a distance of  $r = 1.75$  m, spanning from a polar angle of  $\theta = 65^\circ$  to  $\theta = 145^\circ$ , spaced at a regular interval of  $\theta = 5^\circ$ . The microphone at  $\theta = 90^\circ$  is positioned below the slat. The microphones were calibrated before the tests using a G.R.A.S. 42AA pistonphone calibrator. It is important to note that the beamforming array was removed during the directivity measurements. The microphone arc allows direct measurements of the far-field noise levels as well as the noise directivity for frequencies above  $f = 160$  Hz, corresponding to the cut-off frequency of the anechoic chamber. In order to avoid reflections from the arc itself and noise contamination at mid to high frequencies, the arc is covered in acoustic foam, see Fig. 5.

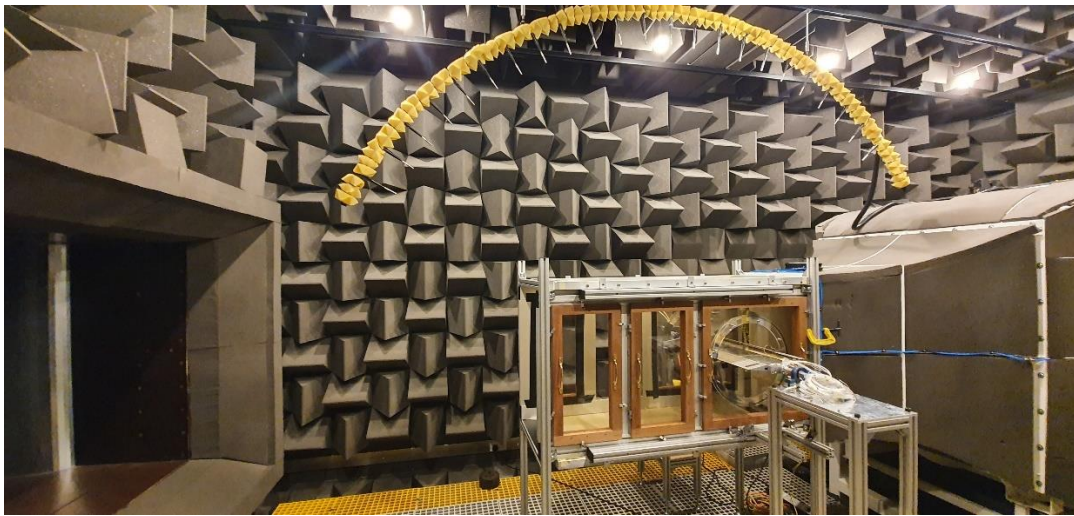


Figure 5: Far-field microphone array used for directivity measurements.

## 2 Results and discussion

In this section, the most relevant results of the tests performed on the DLR F16 model with porous inserts are presented. The test program was intended to investigate the noise reduction potential of the slat with porous inserts applied to the airfoil. This section presents the results under different subsections, starting with the *static pressure* measurements for the baseline and modified porous configurations. In addition to this, *far-field acoustic characteristics*, *near-field surface pressure* measurements, and selected *beamforming* results have also been presented.

### 2.1 Static pressure measurements

This section presents the surface pressure distribution over the baseline and porous configurations in terms of the coefficient of pressure,  $C_p$ . The static pressure measurements were carried out to examine the aerodynamic performance of the airfoil for the baseline configuration (i.e. solid slat) and five modified configurations with porous slat inserts, namely, the DLR-Foam insert, TUD-Fine insert, TUD-Medium insert, TUD-Large insert and TCD-Fabric insert details of which are reported in D2.5. The results are presented in terms of pressure coefficient ( $C_p$ ) and chord normalized streamwise positions  $x/c$  over the high lift device.

The pressure coefficient ( $C_p$ ) results for the baseline configuration are presented in Fig. 6, with the measurements for the slat on the left column and those for the main element on the right column. The tests were performed for the angles of attack,  $AoA = 16^\circ$  (in black),  $18^\circ$  (in red), and  $20^\circ$  (in blue) at the free stream velocity of  $U = 30$  m/s and  $37$  m/s. It is important to note that the airfoil was tested at such high geometric angles of attack since the free-stream angle of attack of the high lift device is expected to be in the order of  $12^\circ$  lower than that of the geometric angle of attack due to the effects of an open-jet wind tunnel. The use of the Kevlar walled test section was expected to reduce these effects. In the present study, the angles of attack for the test campaign were chosen based on the computational studies carried out by ONERA, see Figs. 6a and 6c. The  $C_p$  at the inlet velocity of  $U=30$  m/s and  $U=37$  m/s are shown in Figs. 4 (a & b) and (c & d), respectively. The results for the slat at  $AoA = 6^\circ$  from the computational study compare well with  $AoA = 20^\circ$  from the current test campaign. The final selection of the angles of attack ( $AoA = 16^\circ, 18^\circ, \text{ and } 20^\circ$ ) for this test campaign was based on this comparison.

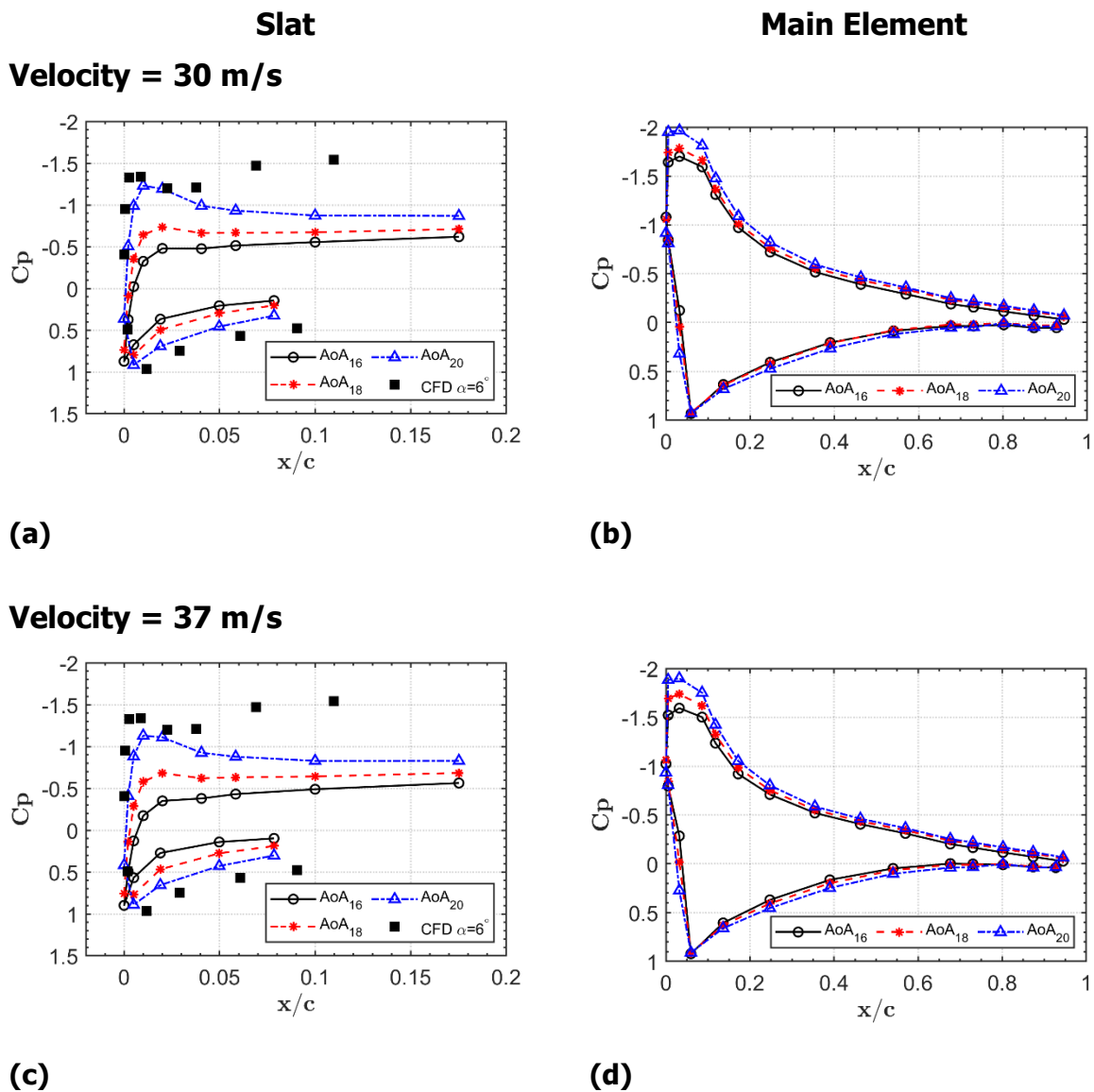
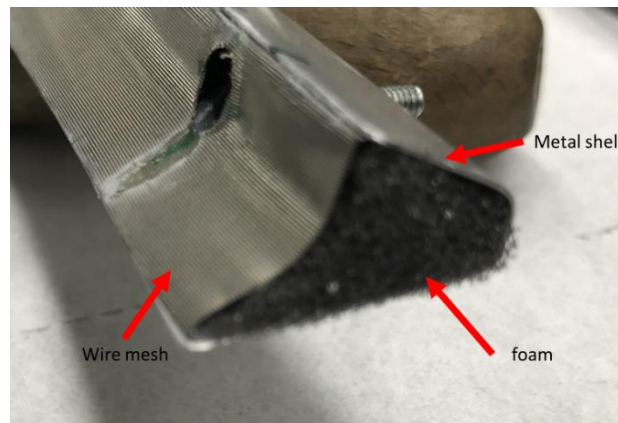


Figure 6: Coefficient of pressure for baseline configuration at  $AoA 16^\circ, 18^\circ, \text{ and } 20^\circ$  for slat (a & c) and the main element (b & d). The results for the slat are compared with the CFD data from ONERA.



According to the results presented for the slat in Fig. 6(a), the suction peak on the upper surface of the slat increases with increasing the angle of attack. As expected, the highest suction peak was found at the highest tested angle of attack,  $\text{AoA} = 20^\circ$ . This trend was observed at a free stream velocity of  $U=30$  m/s. The  $C_p$  at the inlet velocity of  $U=37$  m/s follows a similar trend for the slat as shown in Fig. 6(c).

Further, surface pressure measurements were carried out for the slat fitted with porous inserts. The aeroacoustic characteristics of five different porous inserts were investigated, in-depth detail of which were previously reported in the Deliverable D2.5. The DLR insert assembly is shown in Fig. 7. The DLR-Foam is an open-cell polyurethane foam insert with an inner volume filled with open-cell foam to attenuate unsteady pressures. The wire mesh, covering the DLR-Foam, consists of woven stainless steel and its porosity is about 40%.



**Figure 7: Assembly of DLR-Foam insert.**

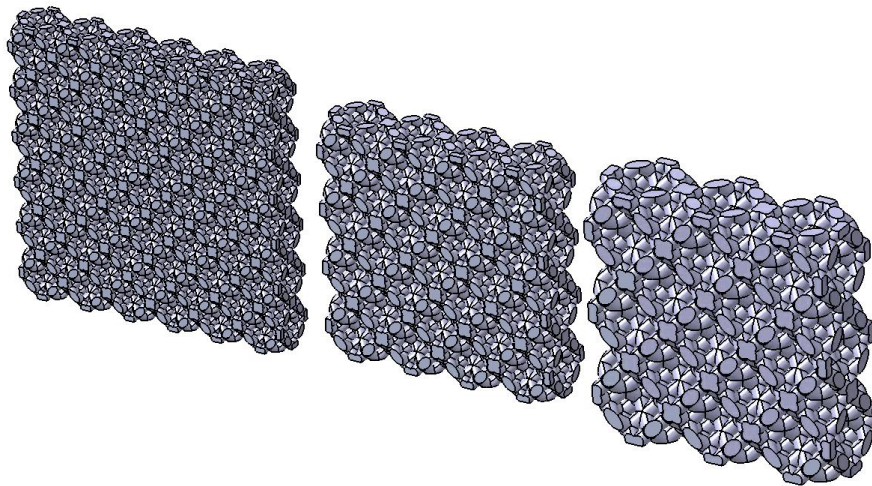


**Figure 8: Isometric view of squared samples. TUD-Fine sample with a cell size of 3.5 mm (left). TUD-Medium sample with a cell size of 4.5 mm (middle). TUD-Large sample with a cell size of 6.5 mm (right).**

Three types of porous slat inserts that were 3D printed by TUD (see Fig. 8), were also tested along with other inserts. These open-cell porous materials were based on the three-dimensional repetition of diamond-lattice unit cells created by scaling the cell size  $d_c$  to 2.5, 3.5, and 4.5 mm. According to their cell size, these porous inserts were named "TUD-Fine", "TUD-Medium", and "TUD-Large" inserts, respectively in the presented results. The porosity of all three micro-structures is 62%. The higher bound for the permeability of the samples is  $10^{-8}$  m<sup>2</sup>. Finally, the test samples of the lattice structures

of the TCD-Fabric with very fine porous structures are shown in Fig. 9, which was printed by TCD as part of the H2020 ARIELIST project.

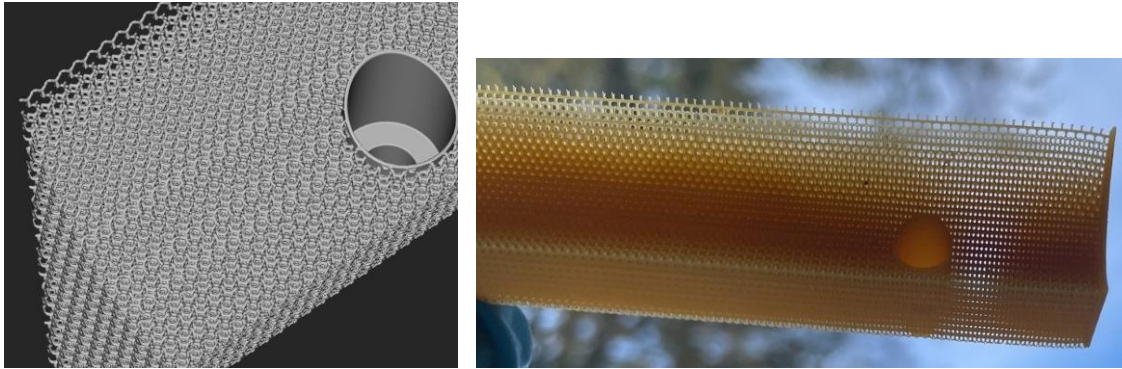


Figure 9: Samples of fine lattice structures printed by TCD.

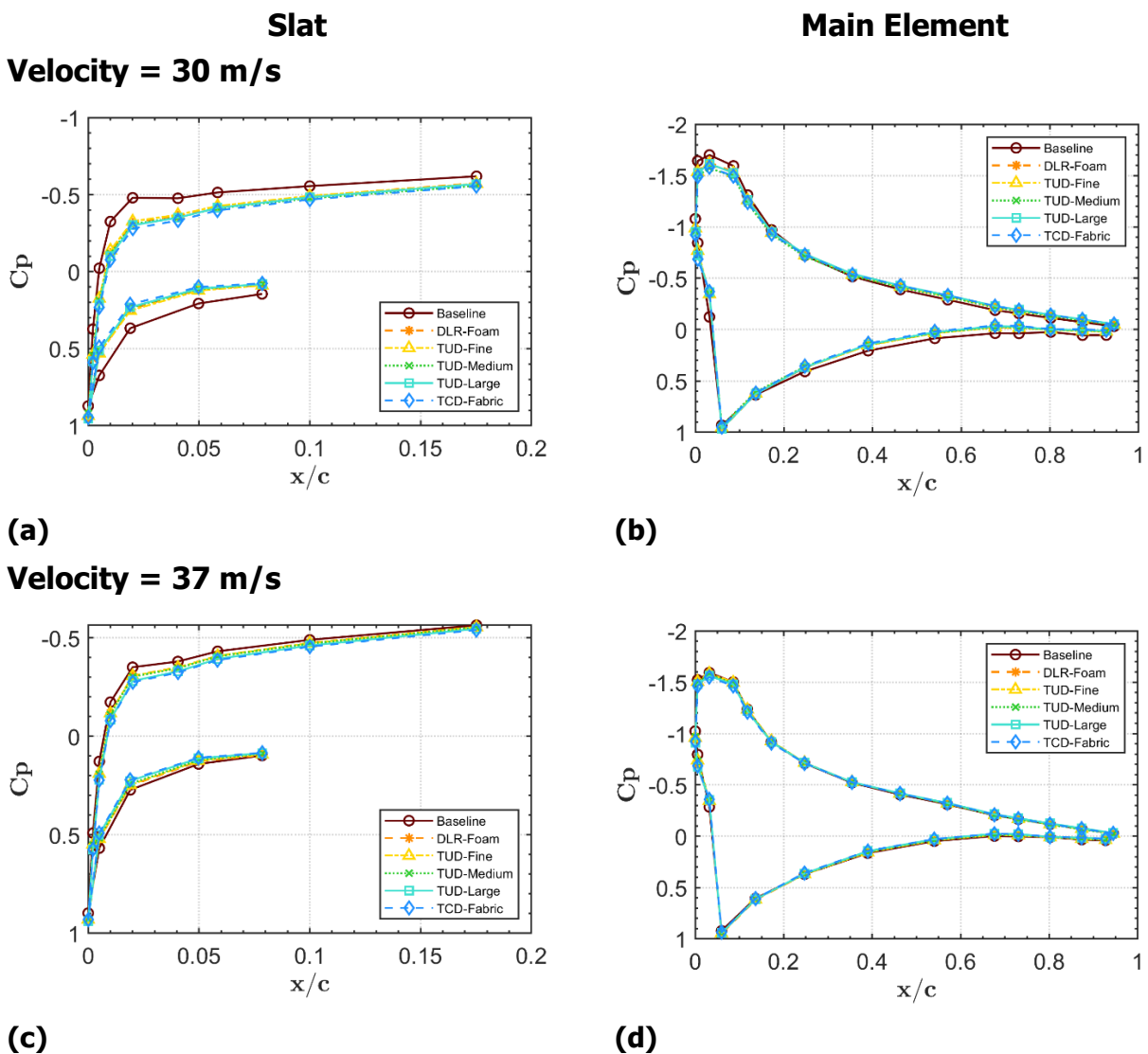
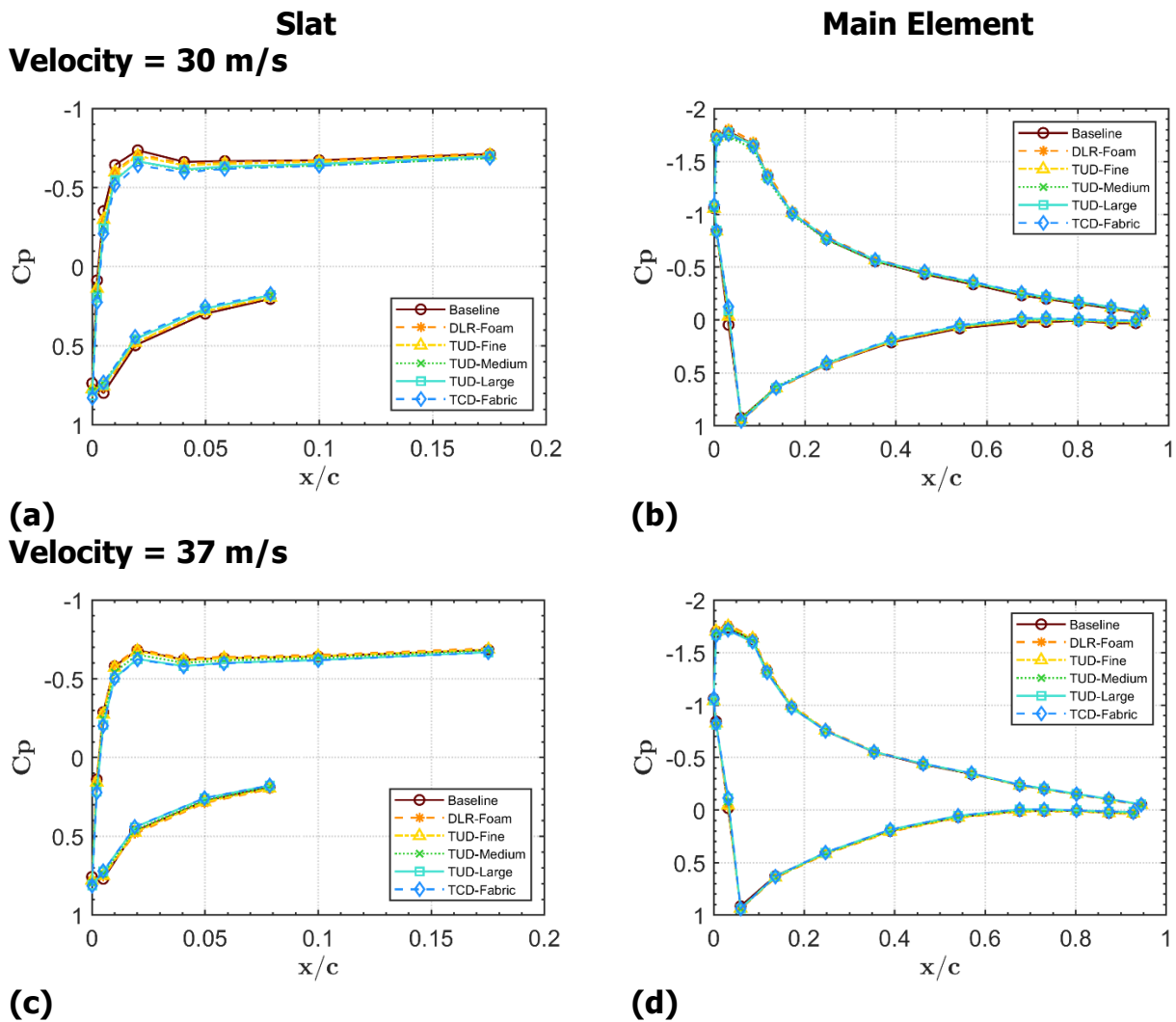


Figure 10: Coefficient of pressure for baseline and treated configurations at AoA = 16° for slat (a & c) and the main element (b & d).

The pressure coefficient results for all the porous-treated configurations, compared with the baseline configuration tested for the angle of attack, AoA = 16°, are shown in Fig. 10. As can be seen from

the presented results in Fig. 10(a), the suction peak for the porous materials has reduced marginally compared to the baseline configuration for the angle of attack,  $AoA=16^\circ$ , at  $U = 30$  m/s. This shows that the slat porous inserts incur only marginal changes in the surface pressure distribution over the treated airfoil. This difference, however, reduces to an unnoticeable value as the free stream velocity increases to  $U = 37$  m/s (see Fig. 10(c)), implying that the slat porous treatment will not have a significant detrimental impact on the aerodynamic performance of the high lift device at high Reynolds number.



**Figure 11: Coefficient of pressure for baseline and treated configurations at  $AoA = 18^\circ$  for slat (a & c) and the main element (b & d).**

As the angle of attack is increased to  $AoA = 18^\circ$  the suction peak obtained for all the tested porous materials is similar to that of the baseline configuration at the velocity of  $U = 30$  m/s as shown in Fig. 11(a). The porous configurations were also tested at the free stream velocity of  $U = 37$  m/s and the  $C_p$  results are shown in Fig. 11(c). As can be seen in the  $C_p$  results, the suction peak obtained for all the tested configurations follow a similar trend to that of the inlet velocity  $U = 30$  m/s (Fig. 11(a)) with minimal difference between the baseline and the treated configurations. As before, the results show that the use of porous slat inserts in the slat does not affect the aerodynamic capability of the tested airfoil. Finally, The  $C_p$  results for the angle of attack  $AoA = 20^\circ$  are presented in Fig. 12. As can be seen, and consistent with the results in Figs. 10 and 11, the porous slat treatments do not

affect the suction peak when compared to the baseline configuration. Based on the results shown in Figs. 10-12, it can be concluded that the use of porous slat treatments does not affect the aerodynamic performance of the tested velocities, even as the angle of attack is increased.

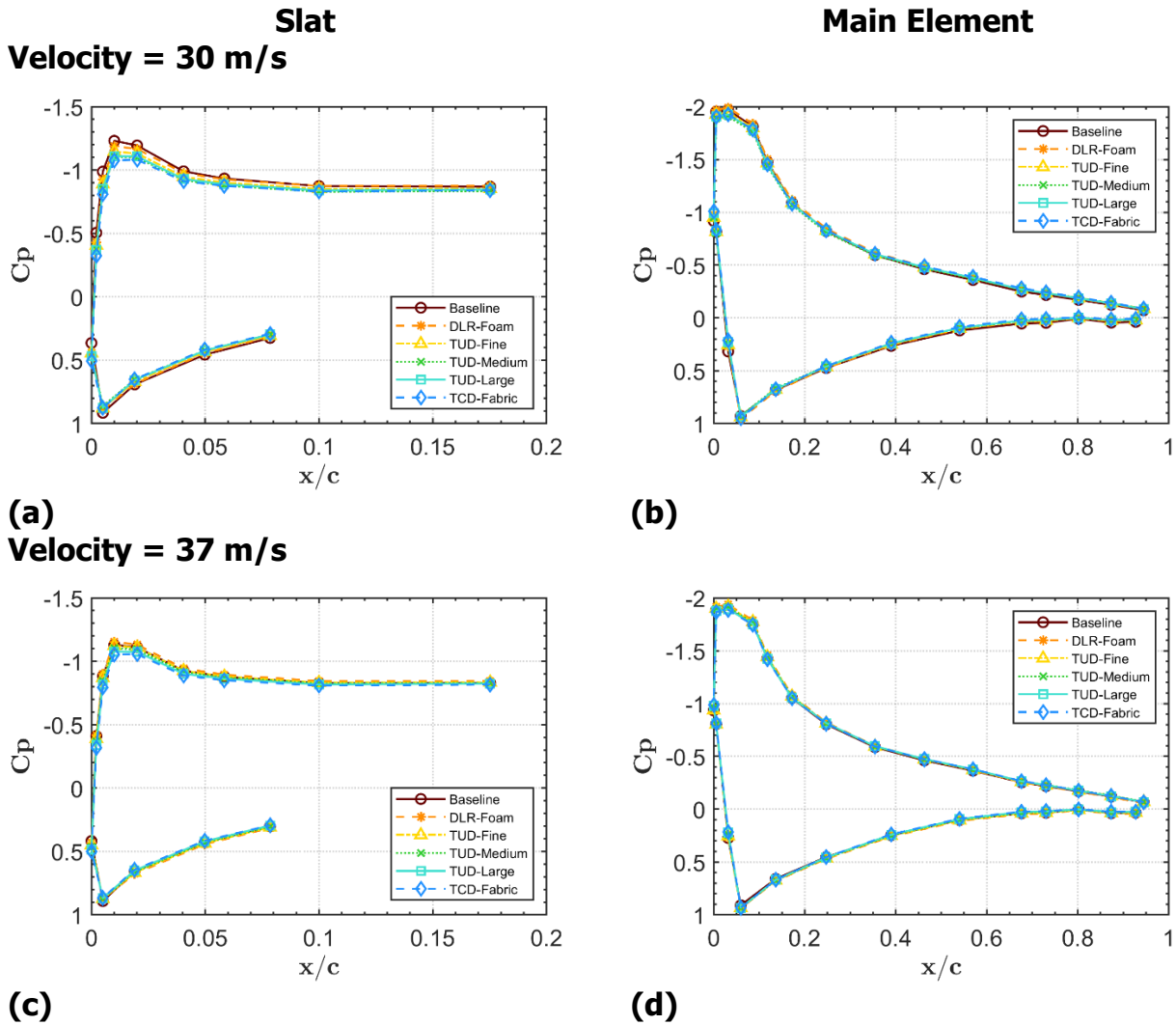


Figure 12: Coefficient of pressure for baseline and treated configurations at AoA = 20° for slat (a & c) and the main element (b & d).

## 2.3 Far-field acoustic measurements

Far-field noise measurements were carried out to assess the noise generated from the porous treatments. The noise measurements were performed on the DLR F16 model for the Baseline, DLR-Foam, TUD-Fine, TUD-Medium, TUD-Large, and TCD-Fabric configurations. The sound pressure level and overall sound pressure level of the far-field and near-field measurements from the tested configurations are presented in this section. The noise measurements were carried out in the open-jet aeroacoustic wind tunnel facility at the University of Bristol fitted with Kevlar walls.

The sound pressure level spectra for the baseline configuration (no porous insert), at three different angles of attack, AoA = 16°, 18°, and 20° are provided in Fig. 13. The SPL was measured from a far-field microphone at 90°, below the slat for the following angles of attack: AoA = 16° (in black), 18° (in red), and 20° (in blue), and are presented for the free-stream velocity of U=30 m/s. Firstly, the results have shown that the SPL for all the angles of attack is 10-15 dB higher than that of the jet

background noise at all frequencies, ensuring accurate measurement of the far-field noise. Furthermore, it can be observed in the presented results that as the angle of attack is increased there is no substantial change in the measured sound pressure levels for the tested baseline airfoil. However, a marginal increase in the order of 2-3 dB at  $f = 300$  Hz to 700 Hz can be observed for the  $AoA=16^\circ$  compared to  $AoA=20^\circ$ . A mild tonal behavior could be observed at about 800 Hz which becomes more dominant at the increasing angle of attack  $AoA=20^\circ$ . Since the results show very similar spectral levels, for brevity the results will further be discussed only for  $AoA=16^\circ$  and  $18^\circ$ .

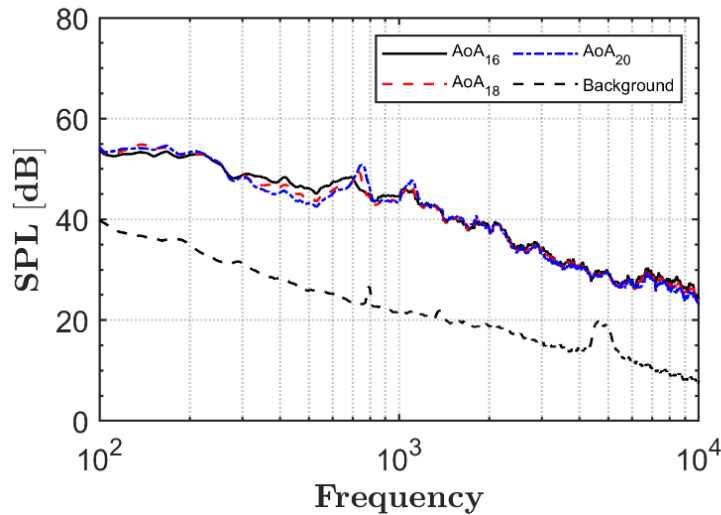
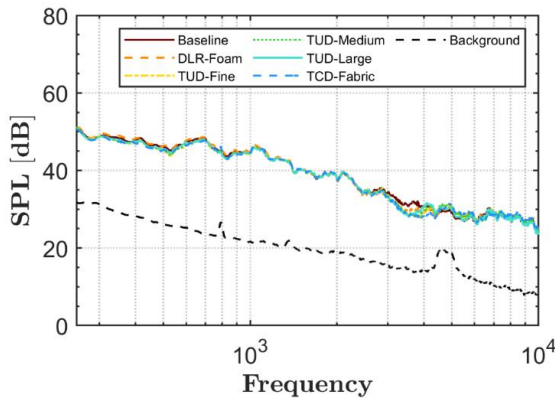
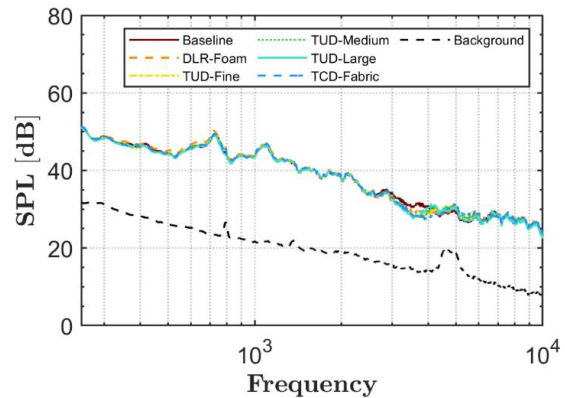


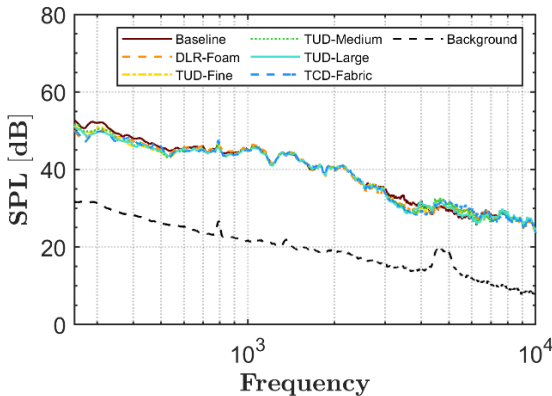
Figure 13: Far-field noise spectra for baseline configuration for  $AoA = 16^\circ, 18^\circ,$  and  $20^\circ$ .



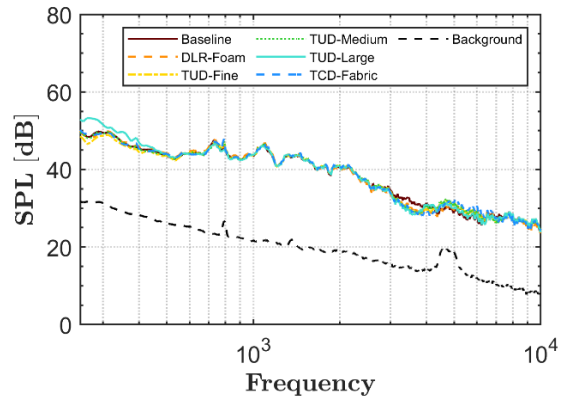
(a)  $AoA = 16^\circ, \theta = 90^\circ$



(b)  $AoA = 18^\circ, \theta = 90^\circ$



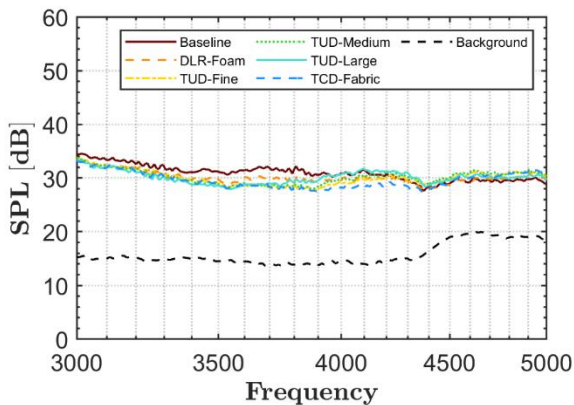
(a)  $AoA = 16^\circ, \theta = 120^\circ$



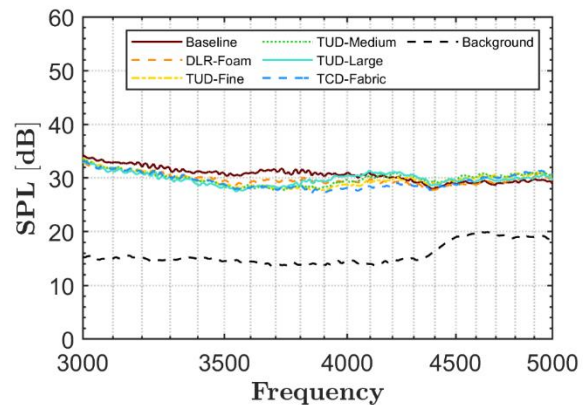
(b)  $AoA = 18^\circ, \theta = 120^\circ$

Figure 14: Far-field noise spectra at  $\theta=90^\circ$  and  $120^\circ$  below the slat at  $U = 30$  m/s for baseline and modified configurations.

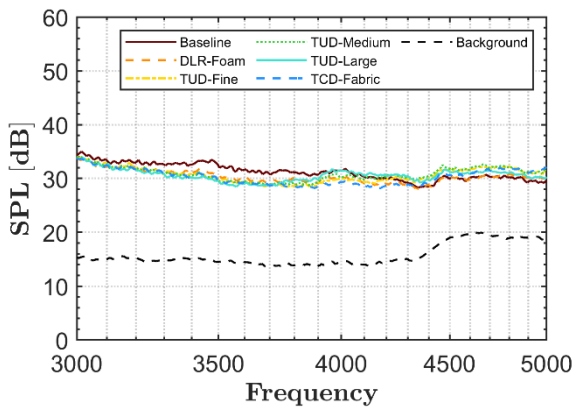
The far-field sound pressure levels for the baseline and all the porous slat treatments are presented for the angles of attack,  $\text{AoA} = 16^\circ$  and  $\text{AoA} = 18^\circ$  in Figs. 14(a,c) and (b,d), respectively. The results are presented for a far-field microphone at  $\theta = 90^\circ$  and  $120^\circ$  below the slat at the free stream velocity of  $U = 30$  m/s. The results presented in Figs. 14 show that the use of porous slat treatments does not contribute to noise reduction and this trend was observed for both the presented angles of attack i.e.,  $16^\circ$  and  $18^\circ$ . The SPL spectra of the treated airfoil are almost the same as that of the baseline (untreated), except for the frequency range of 3000-5000 Hz, where a marginal decrease in noise could be observed. This decrease in the far-field noise for the mentioned frequency range is further investigated to clearly show the distinct noise reduction in the spectra.



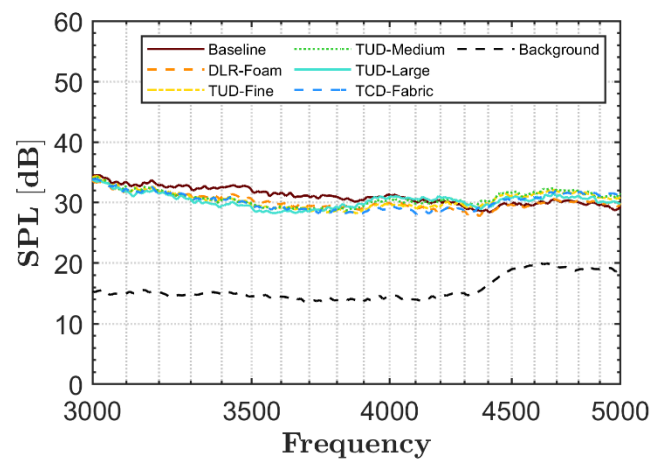
(a)  $\text{AoA} = 16^\circ$ ,  $\theta = 90^\circ$



(b)  $\text{AoA} = 18^\circ$ ,  $\theta = 90^\circ$



(c)  $\text{AoA} = 16^\circ$ ,  $\theta = 120^\circ$



(d)  $\text{AoA} = 18^\circ$ ,  $\theta = 120^\circ$

**Figure 15: Far-field noise spectra at  $\theta = 90^\circ$  and  $120^\circ$  below the slat at  $U = 30$  m/s focused between 3000 and 5000 Hz.**

To discuss the noise reduction achieved for the frequency range of 3000-5000 Hz, the SPL spectra with the adjusted axis are shown in Figs. 15(a,c) for  $\theta = 90^\circ$  and Figs. 15(b,d) for  $\theta = 120^\circ$  the angles of attack,  $\text{AoA} = 16^\circ$ , and  $\text{AoA} = 18^\circ$ , respectively. For the angle of attack,  $\text{AoA} = 16^\circ$  at  $\theta = 90^\circ$ , the use of porous materials in the slat shows a reduction of approximately 2-3 dB in the far-field spectra across the frequency range of 3300-4400 Hz. A noise reduction in the same frequency range can be observed for the same angle of attack,  $\text{AoA} = 18^\circ$  (see Fig. 15(b)). In the case of  $\theta = 120^\circ$  (see Fig. 15(c & d)), the results show noise reduction between 3300-4400 Hz, however, beyond 4400

Hz noise increase for the porous configuration can be seen compared to the baseline except the DLR configuration. All five porous materials show some amount of noise reduction, TCD-Fabric shows the maximum reduction compared to the baseline and other modified configurations, as can be seen in Figs. 15. However, at  $\theta = 120^\circ$  DLR shows the best performance compared to the other porous material. This shows that of all the porous materials used in the slat treatment, DLR-Foam and TCD-Fabric is observed to be slightly more effective in noise reduction for a narrow frequency range between 3000 and 5000 Hz for all the tested angles of attack at  $\theta = 90^\circ$  and  $120^\circ$ .

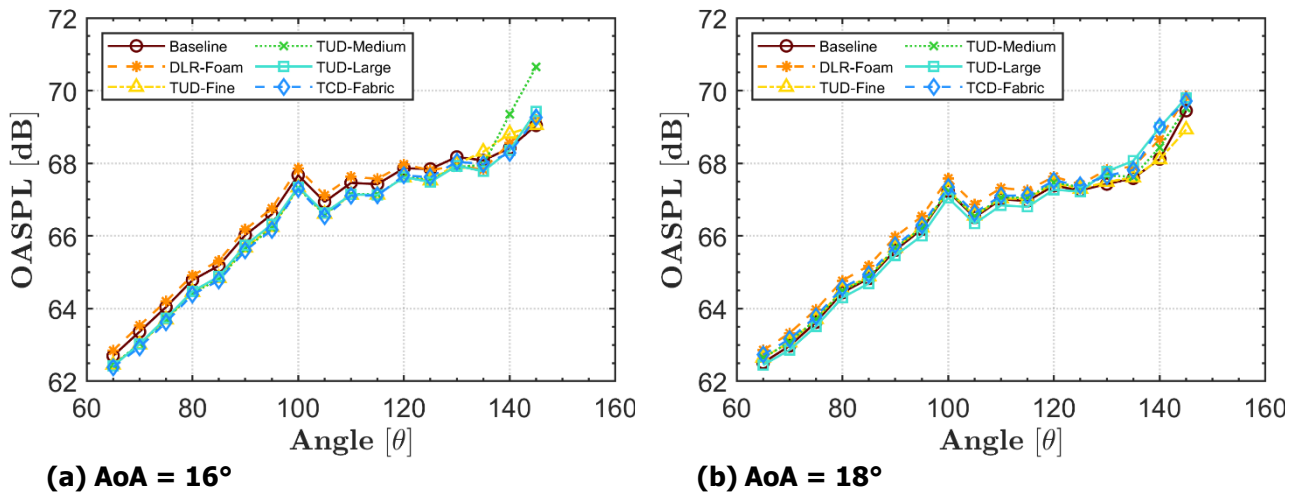


Figure 16: OASPL and directivity measurements for the frequency range of 500 Hz - 10 kHz for (a) AoA =  $16^\circ$  and (b) AoA =  $18^\circ$  at  $U = 30\text{m/s}$ .

The overall sound pressure levels (OASPL) were calculated for the frequency range of 500-10000 Hz and the results for the same are shown in Figs. 16(a) and (b) for the angles of attack, AoA =  $16^\circ$ , and AoA =  $18^\circ$ , respectively. At first glance, it is evident that the porous configurations do not show changes to the OASPL for different directivity angles for all the tested configurations when compared with the baseline (i.e. solid slat), see Fig. 16(a). The observed trend for the OASPL of the baseline is followed by all the other tested configurations through all the directivity angles from  $\theta = 65^\circ - 145^\circ$ . However, the results for the angle of attack, AoA =  $18^\circ$ , shown in Fig. 16(b) TCD-Fabric shows 1-2 dB noise increase in the observed OASPL compared to the baseline.

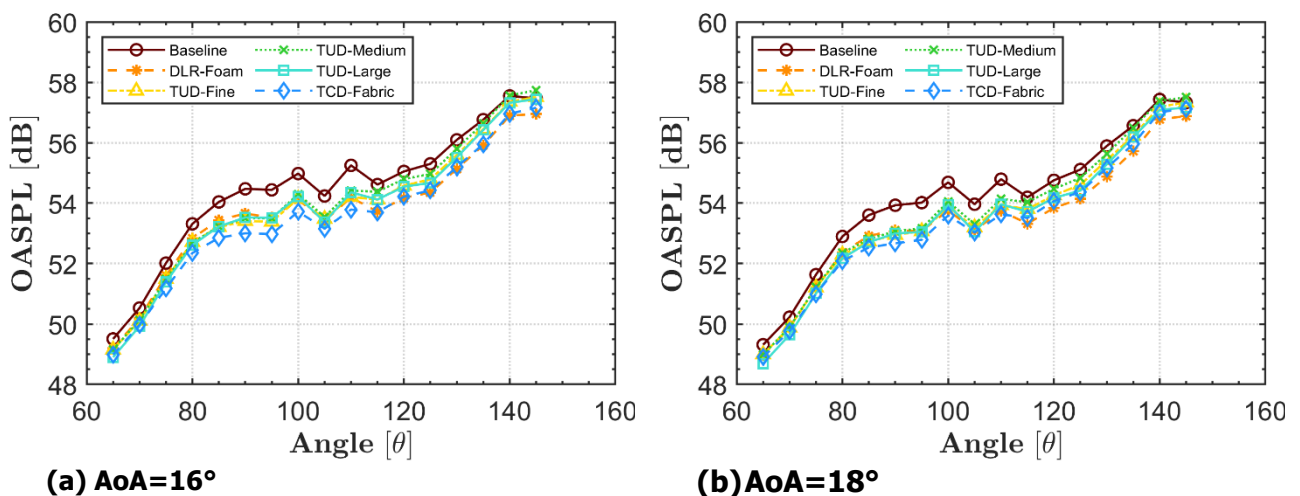


Figure 17: OASPL and directivity measurements for the frequency range of 3 kHz to 5 kHz for (a) AoA =  $16^\circ$  and (b) AoA =  $18^\circ$  at  $U = 30\text{ m/s}$ .

For both the angles of attack, a local peak in OASPL at theta  $\theta = 100^\circ$  could be observed for all the tested configurations. This could be attributed to the direct line of sight for the slat for  $\theta = 100^\circ$  at an increased angle of attack. It was also evident from Figs. 16(a) and 16(b) that for directivity angles between  $\theta = 130^\circ$  and  $145^\circ$  a substantial increase in the OASPL. This increase could be due to the additional noise generated as the flow leaves the Kevlar test section.

The OASPL results for the frequency range of interest from 3 kHz to 5 kHz, where noise reduction was previously observed (see Figs. 14 and 15) for the angle of attack, AoA= $16^\circ$ , and  $18^\circ$  are presented in Figs. 17(a) and (b), respectively. The OASPL results in Fig. 17(a) show that the porous slat treatments result in considerable noise reduction for the directivity angle  $\theta = 80^\circ$  and  $110^\circ$  compared to the baseline configuration. The noise reduction was observed for the mid-frequency range of 3 kHz to 5kHz. Similar acoustic results can be seen for the angle of attack,  $18^\circ$ , as shown in Fig. 17(b). Hence, the data from the acoustic measurements show that the configurations with porous slat treatments are effective in reducing far-field noise at mid-high frequencies. It is important to note that amongst the tested porous inserts, for the frequency range of 3-5 kHz highest levels of noise reduction are shown by the TCD-Fabric at  $\theta < 110^\circ$  and by DLR-Foam at  $\theta > 110^\circ$ . The results show that the treatments with the finest structures show best performance. Therefore, the overall noise reduction for the best-performing cases could be attributed to the absorption levels of the porous material and also the surface roughness of the porous treatments. It is important to note that the overall increase in OASPL past  $\theta = 110^\circ$  could be attributed to the noise increase from the highly deflected flow leaving the Kevlar test section.

## 2.4 Near-field Surface pressure measurements

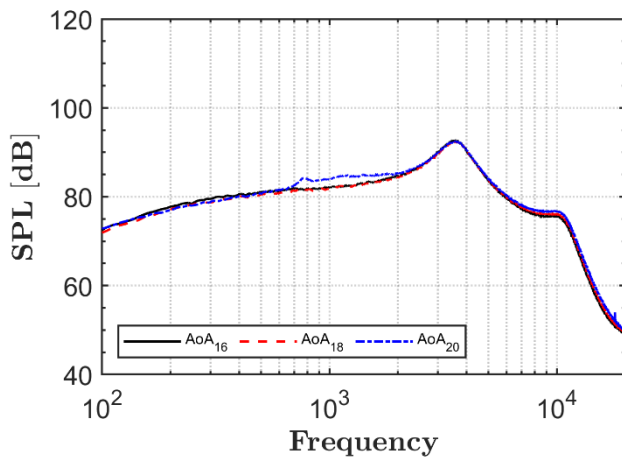
The near-field unsteady surface pressure was measured using sub-miniature piezo-resistive pressure transducers manufactured by KULITE. The slat had insufficient physical space for instrumentation. Therefore, the leading edge of the wing's main element was equipped with 12 Kulite surface pressure transducers. The location on the high-lift device can be found from Fig. 2. As shown in Fig. 2, 8 Kulites are arranged in the chordwise direction on the leading edge of the main element. The second set of 4 Kulites (shown in pink) was distributed in the spanwise direction along the leading edge of the main element, as shown in Fig. 2. The location and spacing of the Kulite ports and a sketch of their position on the airfoil are shown in Fig. 2. The 12 Kulite sensors are referred to as K1, K2, K3, K4, K5, K6, K7, K8, K9, K10, K11, and K12 in the discussions and have been presented in the table on the left in Fig. 18. It is important to note that K1-K5 is positioned past the slat trailing edge over the main element. K6 is located on the leading edge of the main element located within the slat cavity, so it is most relevant to capture slat noise. K7 and K8 are located on the lower side of the main element.

To understand the effects of angle of attack on the near-field surface pressure fluctuation, the SPL results from the Kulites for the baseline configuration (solid slat) at three different angles of attack, AoA =  $16^\circ$  (in black), AoA =  $18^\circ$  (in red), and AoA= $20^\circ$  (in blue) at the free stream velocity of  $U = 30$  m/s are presented in Fig. 18. When considering the sensors K1 and K2 (see Figs. 18(a) and (b)) on the suction side of the main element (see Fig. 2), the SPL results show a characteristic broadband hump between  $f = 2000$ - $3000$  Hz. However, the SPL did not show any difference in magnitude for all three presented angles of attack. The SPL at sensors K4 and K5 located upstream closer to the slat trailing edge shows a similar broadband hump behaviour. Moreover, at K5 the SPL reduces for increasing angles of attack with about 3-4 dB of reduction for AoA =  $20^\circ$  compared to AoA= $16^\circ$ .

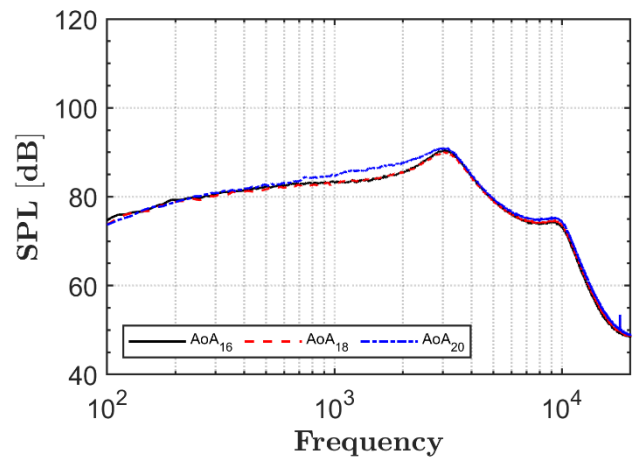




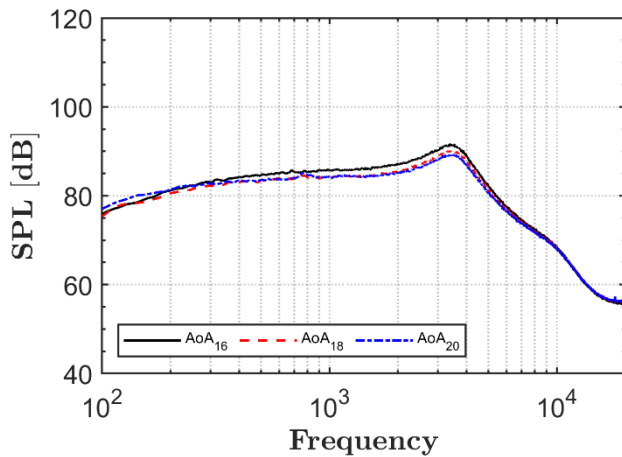
The K6 sensor located on the main-element leading edge within the slat cavity shows a characteristic tonal component at about  $f = 700\text{--}800$  Hz. Studies have shown the tonal component of the slat noise to be due to Rossiter modes. As the angle of attack is increased, the frequency of the tone increases slightly. The mid to high-frequency energy content decreases for the increasing angles of attack compared to  $\text{AoA} = 16^\circ$ . At sensors K7 and K8 on the lower side of the main element (see Fig. 2), the spectra show very dominant tonal characteristics at  $f = 700\text{--}800$  Hz for all three angles of attack. As the angle of attack is increased the tones become more dominant. However, a substantial reduction in the lower frequencies  $f = 200\text{--}700$  Hz can be observed for increasing angles of attack. The spanwise sensors K9-K11 in Fig. 18 show a very similar trend amongst them for the three presented angles of attack with a reduction in the spectra for increasing angles of attack.



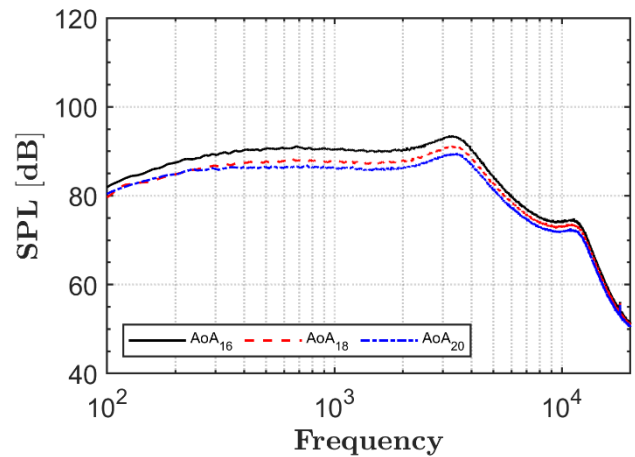
(a) K1



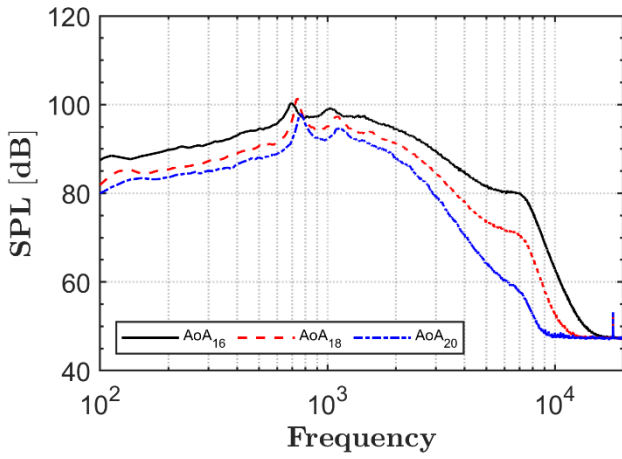
(b) K2



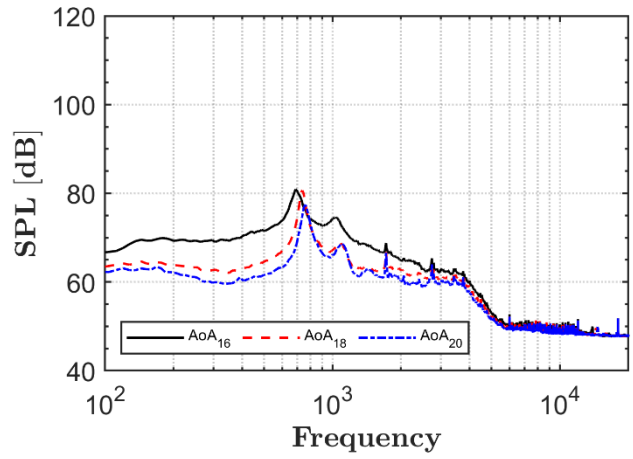
(c) K4



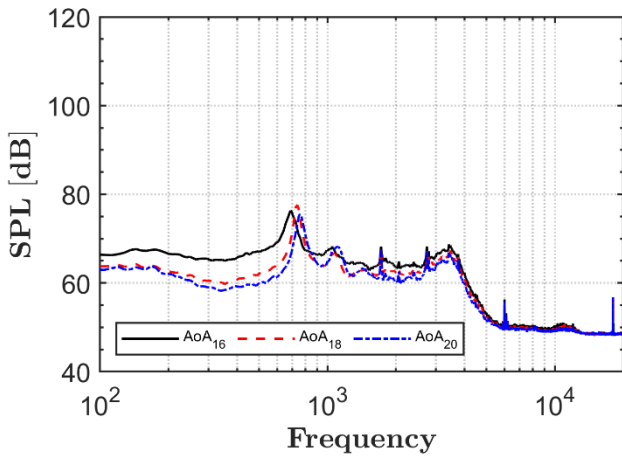
(d) K5



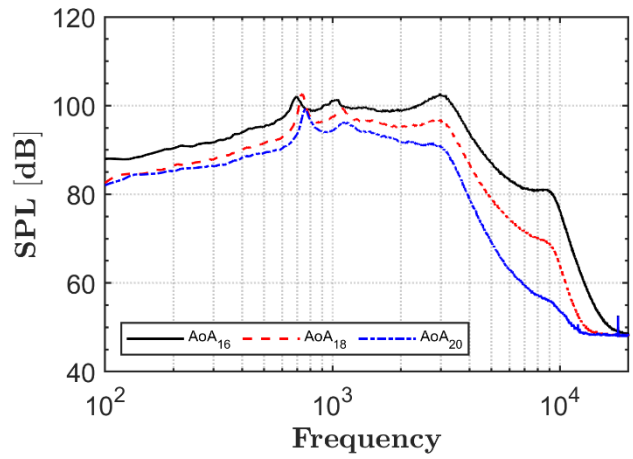
(e) K6



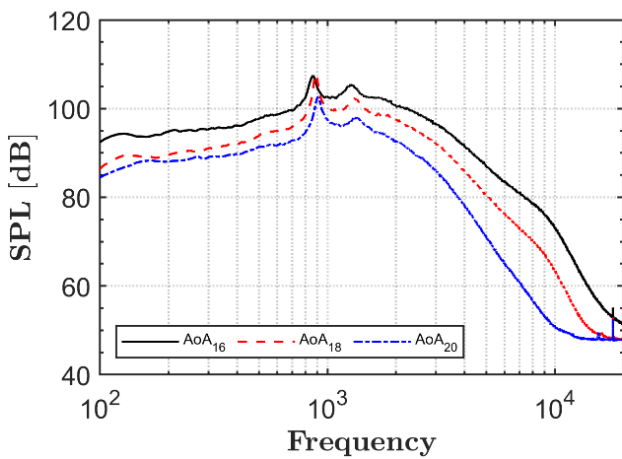
(f) K7



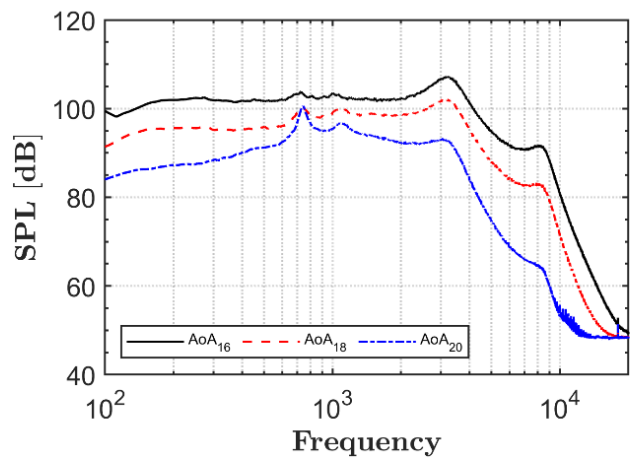
(g) K8



(h) K9

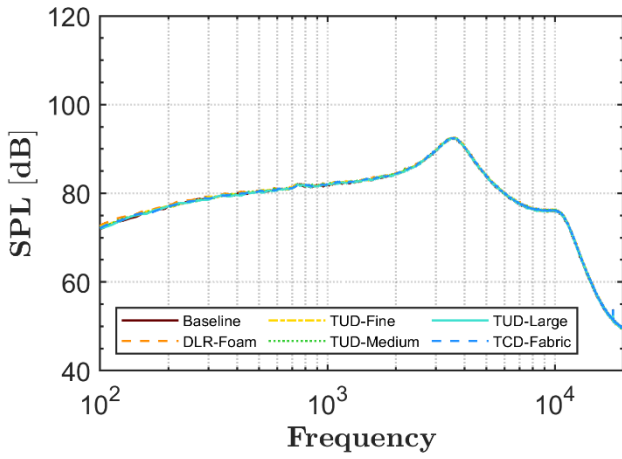


(i) K10

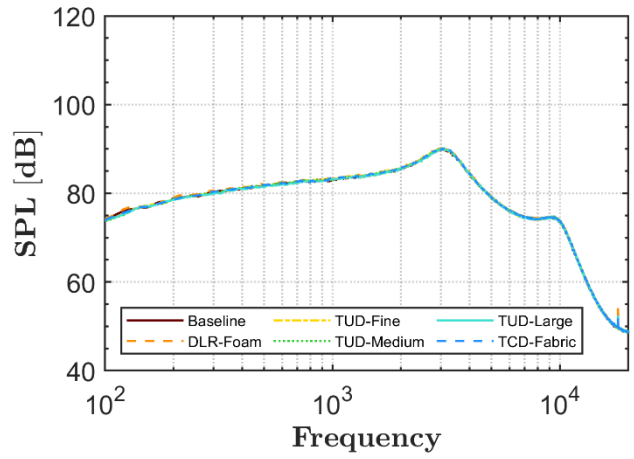


(j) K11

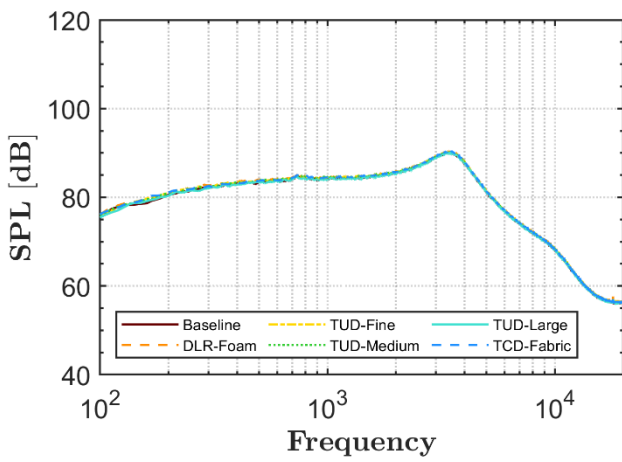
Figure 18: Near-field surface pressure data from Kulites for baseline for increasing angle of attack at U = 30m/s.



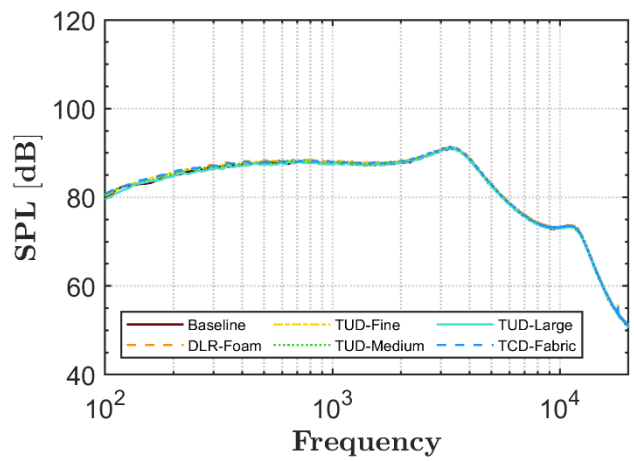
(a) K1



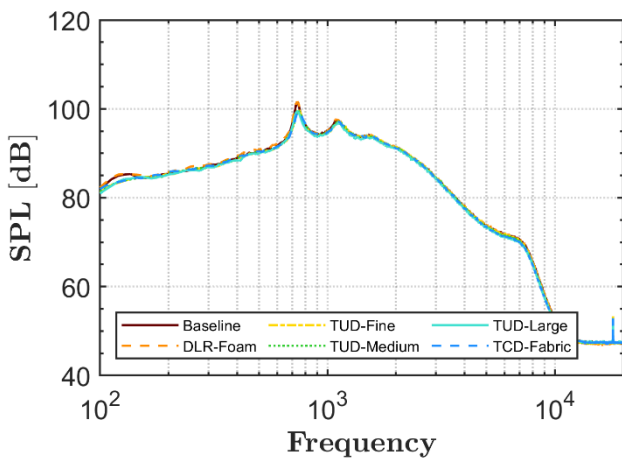
(b) K2



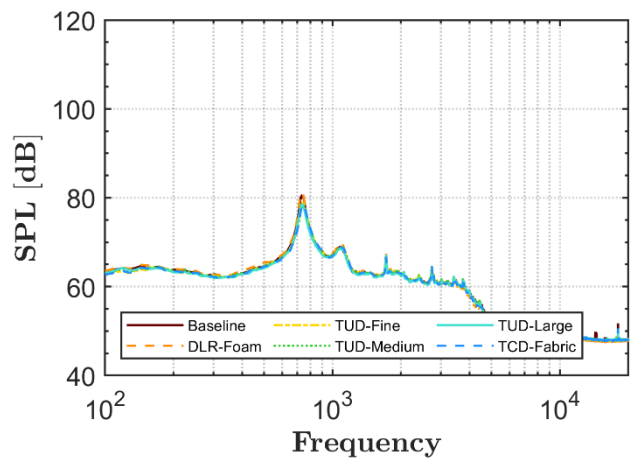
(c) K4



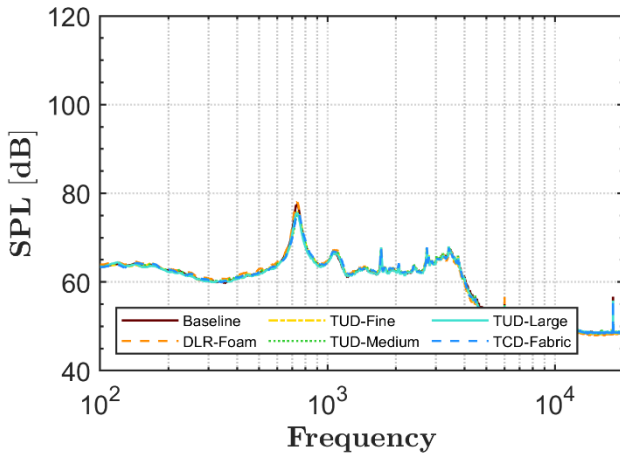
(d) K5



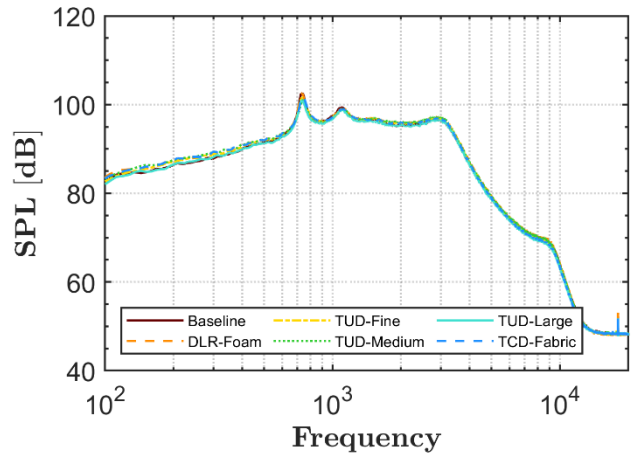
(e) K6



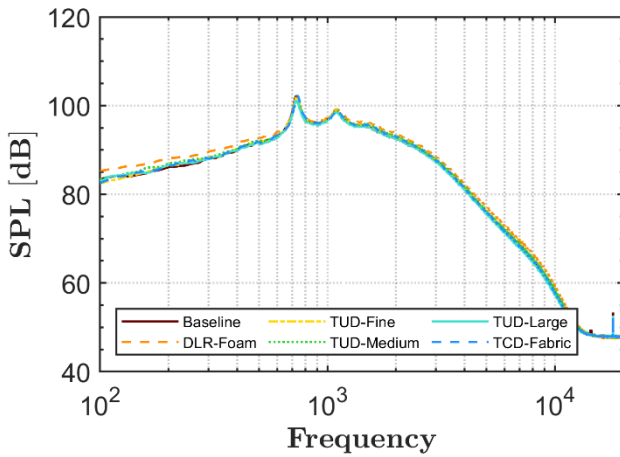
(f) K7



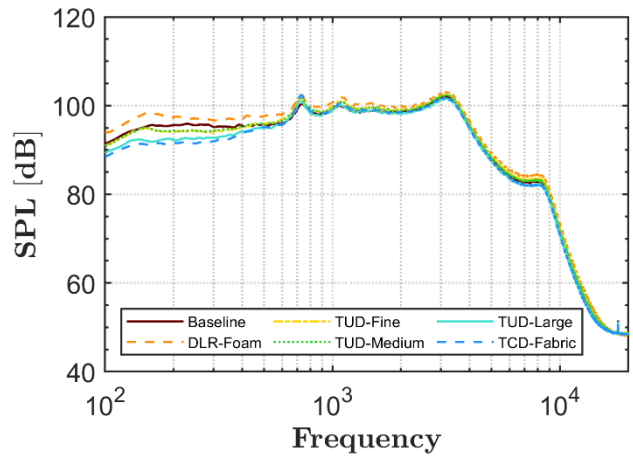
(g) K8



(h) K9



(i) K10



(j) K11

Figure 19: Near-field surface for porous treatment at an angle of attack,  $AoA=18^\circ$  at  $U = 30m/s$ .

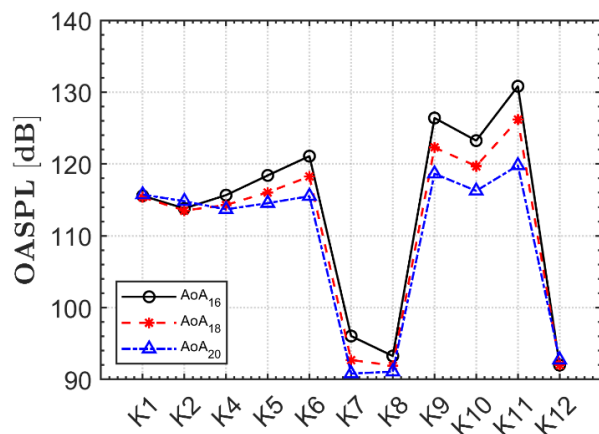


Figure 20: Overall sound pressure level of the surface pressure fluctuations measured using microphones for different angles of attack at  $U = 30m/s$ .

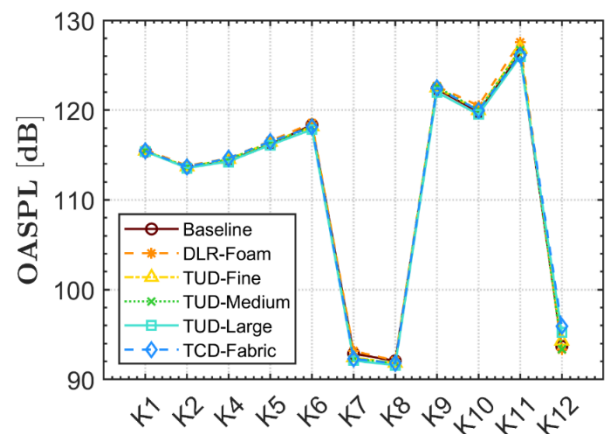


Figure 21: OASPL of near-field surface pressure for porous configurations for  $AoA=18^\circ$  at  $U = 30m/s$ .

The near-field SPL for the baseline and porous configurations (DLR-Foam, TUD-Fine, TUD-Medium, TUD-Large, and TCD-Fabric) at the free stream velocity of  $U=30$  m/s are presented in Fig. 19. For



the sake of brevity, the results are presented for the angle of attack  $AoA=18^\circ$ . As can be seen from Fig. 19, the near-field pressure spectra results for the porous slat configurations do not show any changes compared to the baseline configuration (solid slat), following the spectral trends at sensors K1 to K11 as previously discussed. As demonstrated before in the case of far-field noise, the near-field unsteady pressure data also show that the use of porous slats does not affect the hydrodynamic field within the slat cavity to aid in noise reduction. Therefore, it could be hypothesized that the noise reduction in a narrowband range observed in the far-field noise for the porous configuration could be attributed to the acoustic reflection from the slat cavity.

The OASPL of the near-field unsteady pressure measurements at the locations K1, K2, K3, K4, K5, K6, K7, K8, K9, K10, K11, and K12 (see Fig. 2) at the leading edge of the main element for the baseline configuration (i.e. rigid slat) at  $U=30$  m/s are presented in Fig. 20. The OASPL is presented for the baseline configuration for the tested angles of attack,  $AoA=16^\circ$ ,  $18^\circ$ ,  $20^\circ$ . The results clearly show that the overall sound pressure levels of the unsteady pressure exerted on the body of the lifting device for the baseline case decrease as the angle of attack is increased. Maximum reduction in the spectra was observed for the highest angle of attack,  $AoA=20^\circ$ . Reduction in the spectra of up to 6 dB was observed at the sensor location of K6 within the slat cavity for the angle of attack,  $AoA=20^\circ$ , as can be seen in Fig. 20. Similarly, a reduction in OASPL was also seen for the location K7. The OASPL for the sensors K1, K2, and K3 were almost identical for all three tested angles of attack. Significant reduction of up to 10 dB in the OASPL could be observed at the spanwise distributed Kulite locations of K9, K10, and K11. The OASPL for the porous slat treatments compared to the baseline are presented for the free stream velocity of  $U=30$  m/s at the angle of attack,  $AoA=18^\circ$ . According to the results presented in Fig. 21, the OASPL observed at locations K1-K12 for the different porous configurations was almost identical to that of the baseline configuration. This shows that the use of porous slat treatments for the F16 model did not render any noise reduction.

## 2.5 Beamforming measurements

In the present study, conventional beamforming using the delay-and-sum method was used and a power integration method was used to acquire the source power-integrated SPL. The source power integrated SPL over the region of the airfoil is shown in Fig. 22 for angles of attack,  $AoA=16^\circ$ ,  $18^\circ$ ,  $20^\circ$ . The SPL results are presented in terms of  $1/3^{\text{rd}}$  octave bands. Overall, the results show very similar trends amongst each other with the porous configurations following the same trend as that of the baseline configuration. However, at some mid-frequency ranges between 2-5 kHz the porous configurations show some noise reduction in direct far-field measurements, consistent with our earlier observation using direct microphone measurements, see Figs. 14 and 15. Therefore, to better understand the noise reduction of the porous configurations between 2-5 kHz the beamforming SPL contour maps at 3500 Hz are presented in Fig. 23. This frequency was chosen as SPL from far-field measurements showed the highest level of reduction at this frequency for the porous configuration compared to the baseline. The SPL contours in Fig. 23 show regions with increased levels around the slat region extending along the span of the airfoil. This indicates that the noise reduction for the porous configuration compared to the baseline occurs in the slat region. Therefore, the results indicate that although the porous inserts do not change the hydrodynamic flow field within the slat cavity, they enhance mild noise reduction that possibly occurs due to acoustic reflection.



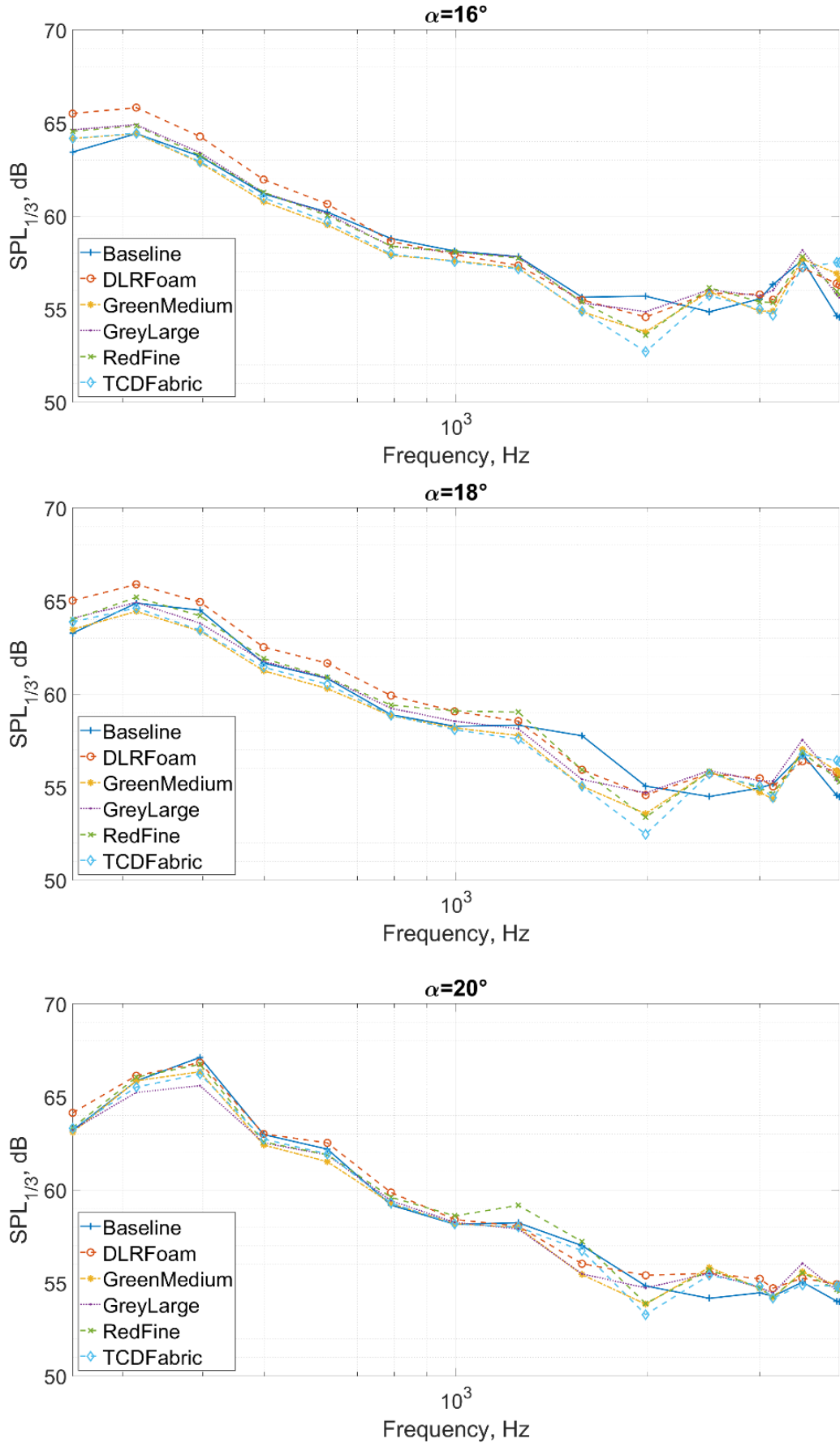


Figure 21- Source power integrated sound pressure level for different porous configurations.



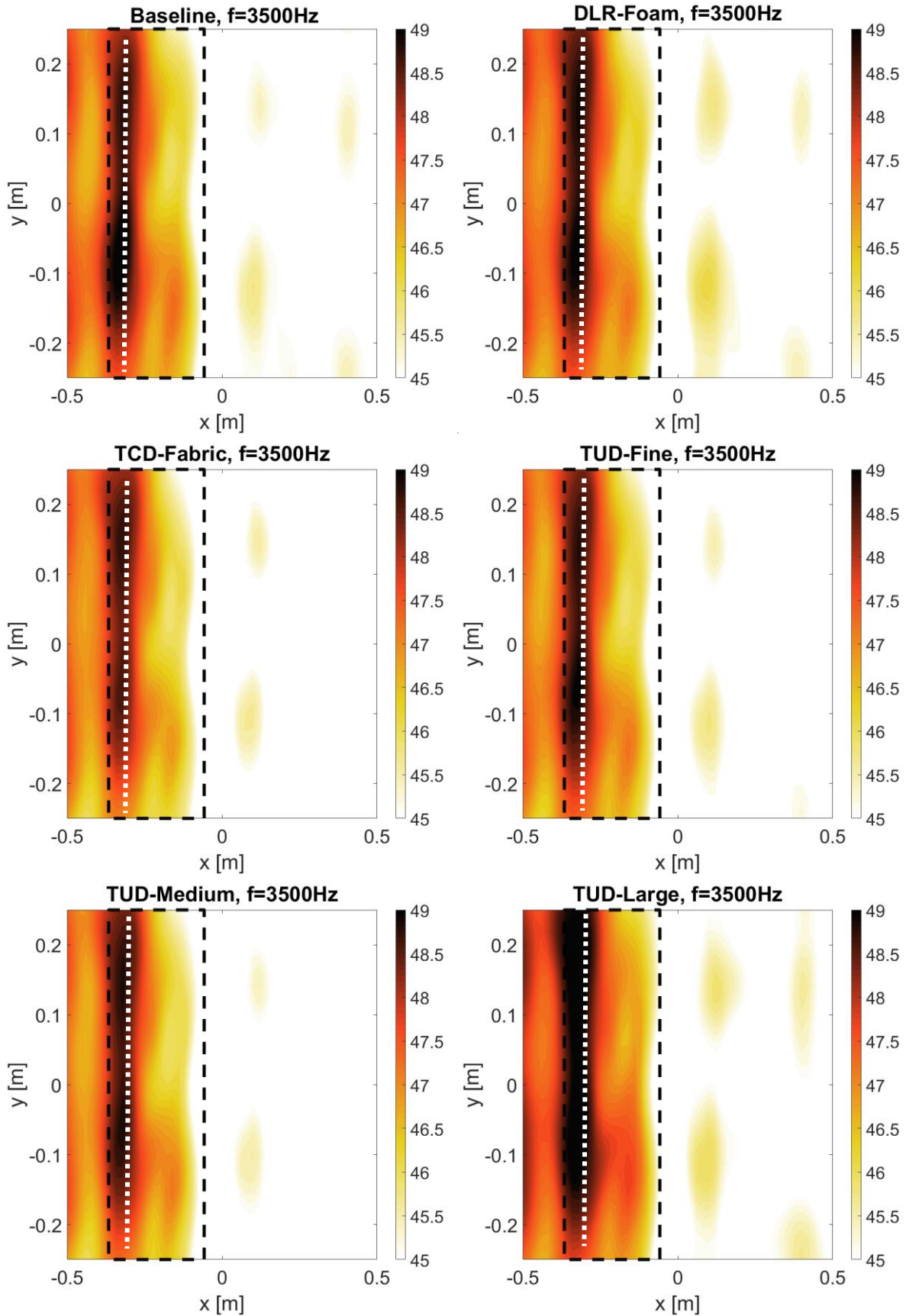


Figure 22 - Beamforming contours for the frequency of interest at  $f = 3500$  Hz, where noise reduction was observed. The black dashed line shows the airfoil outline and the white dashed line shows the slat trailing-edge position.

## 4 Conclusion

Experimental studies were carried out to investigate the aerodynamic and aeroacoustic characteristics of porous slat inserts fitted on DLR's F16 two-element high-lift device with the modified trailing edge. A total of five different porous slat inserts manufactured by TUD, TCD, and DLR were investigated.

The tests were carried out for an angle of attack of  $AoA = 16^\circ$ ,  $18^\circ$ , and  $20^\circ$  at a freestream velocity of  $U = 30$  m/s and  $U = 37$  m/s. The results of the pressure coefficients did not show any changes in the suction peak compared to the baseline configurations, demonstrating that the porous slat inserts had a very minimal effect on the aerodynamic performance of the high-lift device.

The sound pressure level for the baseline did not show any difference among the tested three angles of attack  $AoA = 16^\circ$ ,  $18^\circ$ , and  $20^\circ$  for both the tested inflow conditions. The porous slat inserts showed a significant reduction in the noise levels at about  $f = 3000 - 5000$  Hz compared to the baseline condition. The TCD foam showed the best performance amongst the tested porous inserts at  $\theta < 110^\circ$  and the DLR-Foam showed good performance at  $\theta > 110^\circ$ .

The near-field measurements showed a characteristic tonal hump for the baseline configuration for all the tested angles of attack with the highest levels of spectra for the  $AoA = 16^\circ$ . The near-field spectra of the porous slat inserts did not show a difference compared to the baseline configuration at all the tested angles of attack.

The sound pressure level contours from the beamforming measurements showed increased levels around the slat region extending along the span of the airfoil. This indicates that the noise reduction for the porous configuration compared to the baseline occurs in the slat region. Overall, the results indicate that although the porous inserts do not change the hydrodynamic flow field within the slat cavity, they enhance noise reduction.